AIAA JOURNAL
Vol. 49, No. 8, August 2011

Active Separation Control with Pulsed Jets in a Critically Loaded Compressor Cascade

M. Hecklau,* O. Wiederhold,† V. Zander,‡ R. King,§ and W. Nitsche¶
Berlin Institute of Technology, 10587 Berlin, Germany
and
A. Huppertz** and M. Swoboda††
Rolls-Royce Deutschland Ltd & Co KG, 15827 Dahlewitz, Germany

DOI: 10.2514/1.J050931

In this contribution the impact of active flow control by means of pulsed blowing in a critically loaded compressor cascade will be described. Because of the high loading of the blades, a fully three-dimensional and complex flowfield is developing. Experimental investigations with active flow control were undertaken to increase the turning and the pressure rise of the stator cascade, by suppressing separation phenomena in the passage flowfield. Two different concepts of actuators were used. First, pulsed blowing out of the endwalls was used to reduce the secondary flow structures. Second, the flow was excited with actuators flush-mounted on the blade's suction surface. The best performance was reached by using both actuator concepts in combination. A multivariable closed-loop control approach was used to control both separation phenomena simultaneously. Heavy disturbances could be compensated and a stabilization of the cascade operation point was achieved.

I. Introduction

FLOW control applications in turbomachinery have a great potential to break fundamental barriers [1], like the aerodynamic loading on the compressor blades that limits the performance of the axial compressor. Generally, these parts are conservatively designed, with a certain margin to the stall boundary, preventing unstable compressor operation. With active flow control (AFC) devices the pressure ratio of one compressor stage can be increased by enhancing the turning of the stator blade to a critical level. Reaching the same overall pressure ratio of the compressor permits to reduce the number of stages of an axial compressor. This leads to a reduction in weight and size of the compressor, which could be one way to decrease manufacturing and operational costs of axial turbomachinery in the future [2].

In the past, different AFC methods have been investigated by Culley et al. [3] in an axial compressors facility with the focus on boundary-layer separation on highly loaded stator blades. Even with a significantly decreased actuator mass flow they reported a significant reduction of the total pressure loss in [4]. Bright et al. [5] performed in a full-annulus experiment a closed-loop separation control approach, using steady injection along 42 stator blades. Passive and active flow control applications, with the focus on boundary-layer separation and secondary flow structures, were tested in several ways, mostly on linear stator cascades [6–8]. Experimental and numerical investigations of steady-state methods for controlling strong secondary flow structures as well as boundary-layer separation were presented by Nerger et al. [9]. The pressure rise across the stator passage was significantly increased and the total pressure loss reduced. To achieve this, a mass flow of up to 3% of the passage flow was required. With periodical addition of momentum the cost could be decreased by an order of magnitude comparable to that of steady blowing [10,11].

A compressor cascade with critically loaded stator blades was used for the present investigation. Because of the critical loading and the low aspect ratio of the blades, a fully three-dimensional and complex flowfield with boundary-layer separation is developing [12]. AFC devices are used to enable the overcritical turning of the blades by preventing the boundary layer to separate on the blade's suction surface. For the project presented, actuators with periodic excitation are used [13,14]. First, pulsed blowing out of the sidewalls is used to reduce the secondary flow structures. Secondly, the flow is excited with actuators mounted on the suction side. In a final step, both actuator concepts are operated in combination with selected amplitudes and frequencies [15].

Moreover, a closed-loop control approach is suggested to control both separation phenomena simultaneously. By definition of two real-time accessible control variables a multiple-input multiple-output (MIMO) control task [16] can be derived. An optimal H_∞-control approach [17] for the MIMO case is suggested to control the dominant separation phenomena at the same time. It is demonstrated that closed-loop control enables stable operating conditions even under heavily disturbed circumstances.

II. Experimental Setup

A. Cascade Test Rig

A stator compressor cascade in a low-speed cascade test rig was used for the experimental investigations. Rolls-Royce Deutschland provided the cascade and stator blade geometry as the industrial partner. The blades are designed with an overcritical turning and a low aspect ratio of AR = 0.8. As shown in Fig. 1a, the cascade consists of seven blades. The cascade is mounted on rotatable disks, which enables a continuous change of the inflow angle β_1 to change the aerodynamical loading on the stator blades. For the design point

Presented at the 5th Flow Control Conference, Chicago, IL, 28 June–1 July 2010; received 28 September 2010; revision received 18 January 2011; accepted for publication 1 February 2011.

*Research Assistant, Department of Aeronautics and Astronautics, Chair of Aerodynamics; martin.hecklau@ilr.tu-berlin.de.
†Research Assistant, Department of Process Engineering, Chair of Measurement and Control; olaf.wiederhold@tu-berlin.de.
‡Research Assistant, Department of Aeronautics and Astronautics, Chair of Aerodynamics; vincent.zander@ilr.tu-berlin.de.
§Professor, Department of Process Engineering, Chair of Measurement and Control; rudibert.king@tu-berlin.de.
¶Professor, Department of Aeronautics and Astronautics, Chair of Aerodynamics, wolfgang.nitsche@tu-berlin.de
**Graduated Research Engineer, Design Systems Engineering, andre.huppertz@rolls-royce.com
††Graduated Research Engineer, Design Systems Engineering, marius.swoboda@rolls-royce.com

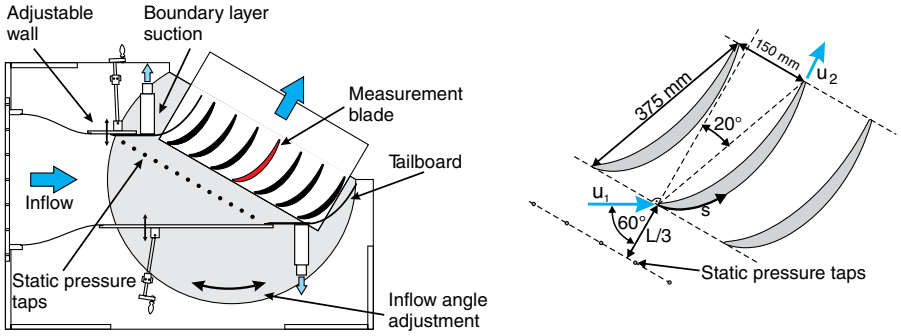

a) Cascade test rig **b) Cascade geometry**

Fig. 1 Schematics of the compressor cascade with a blade height of $h = 300$ mm.

of $\beta_1 = 60°$ the test section dimension of the inlet are 525 by 300 mm. A homogeneous cascade inlet flow is achieved by two additional tailboards and boundary-layer suction at the end of the horizontal endwalls. At each sidewall 14 static pressure taps are installed for monitoring the inlet flow uniformity. To obtain a sufficient thickness of the blade for the integration of active flow control devices inside the blade, the geometry of the cascade is scaled up, as shown in Fig. 1b. The cascade test rig is operated in an open wind tunnel. The design inlet flow speed of $u_1 = 34$ m/s is used for this investigation. The corresponding Mach number for the design case is $Ma = 0.1$ and the turbulence intensity is $Tu = 2.1\%$ at the cascade inlet. Based on the blade chord length, the Reynolds number is $Re_L = 8.4 \cdot 10^5$.

B. Actuator System

According to the complex flow separation in the passage flowfield, the AFC approaches had to be adapted to the dominant flow features. For that reason each passage of the cascade is equipped with two different actuator systems. In both actuators periodic excitation of compressed air is used.

1. *Sidewall Actuators (SW)*

Pulsed blowing out of slots integrated in the cascade sidewalls is used as an active method of controlling the dominant secondary flow structures. For this purpose, the air is blown through slots at a chord length of $x/L = 10\%$, as can be seen in Figs. 2a and 2b. In the experiment, the slot's geometry is 20 mm in height and 0.4 mm in width. In numerical investigations [18,19] several actuator parameters have been studied, such as the injection angle, the injection amplitude, and the actuator position. According to these numerical investigations, the injection angle in main flow direction to the sidewall is set to 15°. For symmetrical flow conditions while actuating, all passages of the cascade are equipped with actuators at both sidewalls.

2. *Blade Actuators (BA)*

The flow separation on the suction surface of the blade is suppressed by actuators installed inside the stator blade. The actuator orifice is positioned upstream of the separation line at 66.5% of the blade's chord. The actuator system consists of three slot-segments, which can be addressed individually cf. Fig. 2a, with the middle segment BA2 and the outer segments BA1 + 3. The slots are orientated in spanwise direction and have a geometry of 50 mm in length and 0.4 mm in width. Between the segments the distance is kept as small as possible, resulting in a separation of 2 mm. The wall jet has a blowing angle of 45° to the local blade surface (cf. Fig. 2c). Because of the shape of the actuator cavity, a uniform velocity distribution in spanwise direction can be achieved.

3. *Excitation Setup*

Fast-switching solenoid valves (*Festo, MHE2* with a switching frequency up to 250 Hz) are used for pulsing the compressed air in both actuator concepts, by variation of frequency and duty cycle. The complete actuator assembly installed in the cascade test rig for open-loop control experiments is displayed in Fig. 3. The excitation setup is divided into three actuator circuits, one for the sidewall actuators and two for the blade actuators. Each actuator circuit has a pressure supply system, consisting of a mass flow meter, a pressure control valve, and a pressure distributor. The mass flow of air passing through one actuator circuit is measured by the mass flow meter (*Bronkhorst, F-203AC* with an accuracy of ±1%). The amplitude is controlled by the pressure control valve (*Festo, MPPE*), providing a

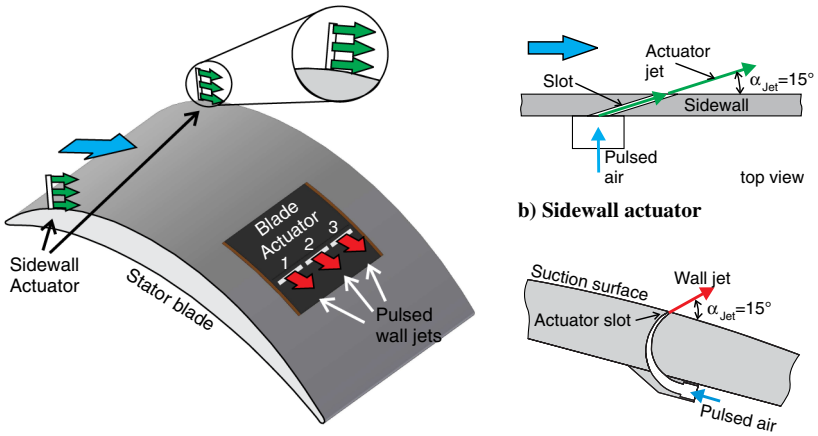

a) Stator blade with actuator setup **b) Sidewall actuator** **c) Blade actuator**

Fig. 2 Schematics of a) stator blade with sidewall actuator and the wall jet of the blade actuator, b) slot geometry and jet angle of the sidewall actuator (cross section in top view), and c) actuator chamber and jet angle of the blade actuator (cross section).

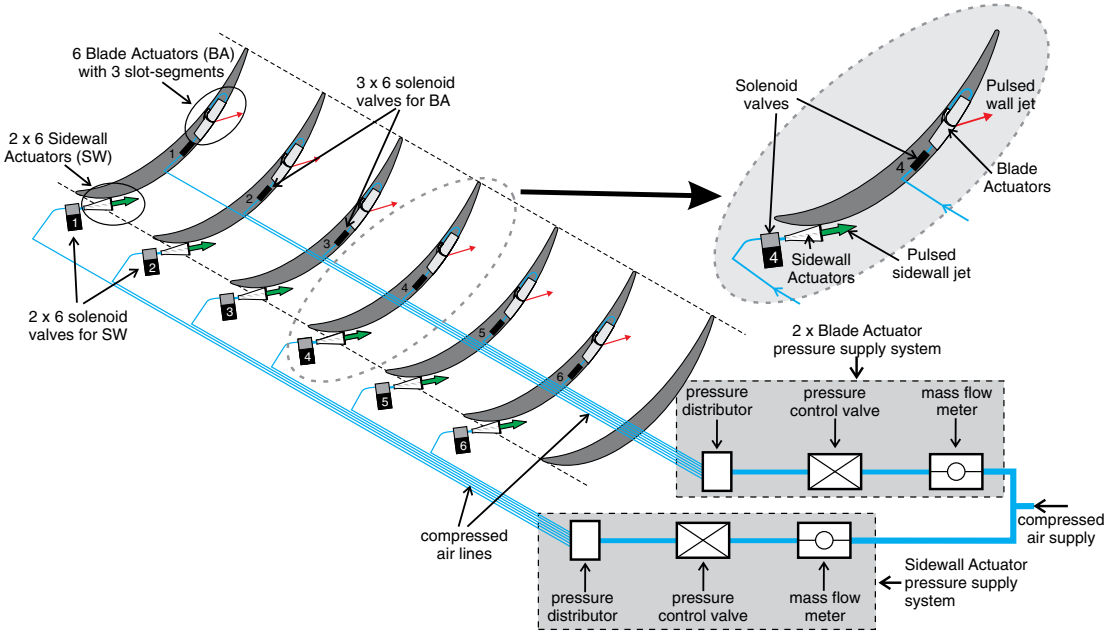

Fig. 3 Assembly of the blade and sidewall actuator systems.

certain pressure in the pressure distributor. The solenoid valves of one circuit are connected to this pressure distributor, each with the same length of the compressed air lines.

The sidewall actuator setup consists of 12 solenoid valves. The valves are directly connected to the actuator chamber, since the jet velocity and the signal quality of the pulse is highly influenced by the volume between the valve and actuator orifice. The actuator chamber decelerates the compressed air flow and converts the circular cross section of the pressure pipe to the rectangular actuator slot.

The blade actuators are integrated with the solenoid valves in the stator blades. Each slot-segment is equipped with one solenoid valve, resulting in a total of 18 valves for the blade actuators. As described before, this actuator setup is divided into two pressure circuits, one for the outer slot-segments (BA1 + 3) and one for the middle slot (BA2).

This actuator setup enables individual adjustment of the amplitude and mass flow for each pressure circuit, like the sidewall actuators (SW), the middle slot-segments of the blade actuators (BA2), and the outer segments (BA1 + 3). The actuators were calibrated by hot-wire measurements of the jet velocity along the actuator slot. The blowing momentum coefficient c_μ was obtained for each actuator system individually, resulting in a look-up table (LUT) for each forcing frequency and duty cycle. The response of the wall jet to the trigger signal is slightly dependent on the forcing frequency. The jet velocity has a steep rising and falling edge, without constant flow during the off-cycle, e.g., due to leakage of the solenoid valve. With increased forcing frequency the falling edge becomes more slanted, resulting in a shift of the effective duty cycle to enlarged values. The response time of the jet velocity to the trigger signal is between 1.6 and 2 ms. More details about the actuator characteristics are summarized in [15]. As an example, in Fig. 4 the LUT of both actuator concepts is given for two forcing frequencies and a duty cycle of DC = 50%. Thereby the values for the blade actuator segments are summed up, denoted as BA, as in the later presented closed-loop control experiments the three blade actuator segments are used as one actuating unit. The data described represent actuation with blowing ratios of $3.0 \leq u_{\text{jet,max}}/u_1 \leq 4.0$ for the sidewall actuators (SW) and $0.9 \leq u_{\text{jet,max}}/u_1 \leq 2.8$ for the blade actuators (BA). The momentum coefficient represents the amplitude of the actuator with the injected mass flow $\dot{m}_a$, the average actuator jet velocity $\bar{u}_{\text{jet}}$, the dynamic pressure at the cascade inlet q_1, and the area of the cascade inlet plane F_1:

$$c_\mu = \frac{\dot{m}_a \cdot \bar{u}_{\text{jet}}}{q_1 \cdot F_1} \tag{1}$$

For unsteady excitation, the forcing frequency is normalized by the quotient of a geometrical reference length and a reference velocity. In this context, the blade chord L is used to normalize the actuator frequency. With the inflow velocity u_1 the reduced forcing frequency is calculated as:

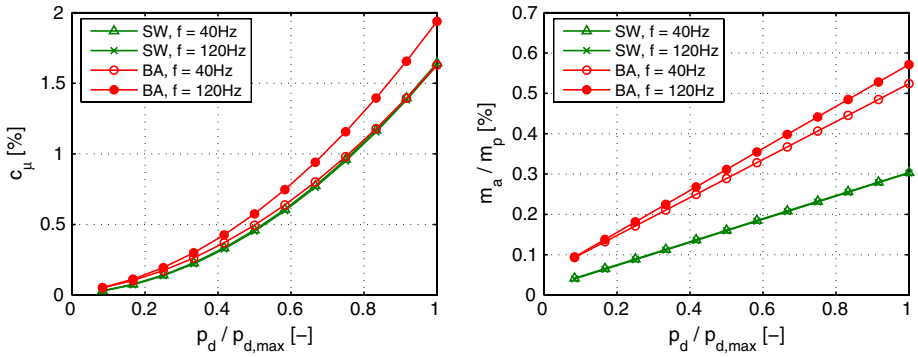

Fig. 4 LUT with the dependency of the actuator momentum and injected mass flow, respectively, to the supplied pressure in the pressure distributor p_d, with $p_{d,\text{max}} = 6$ bar and a duty cycle of DC = 50%.

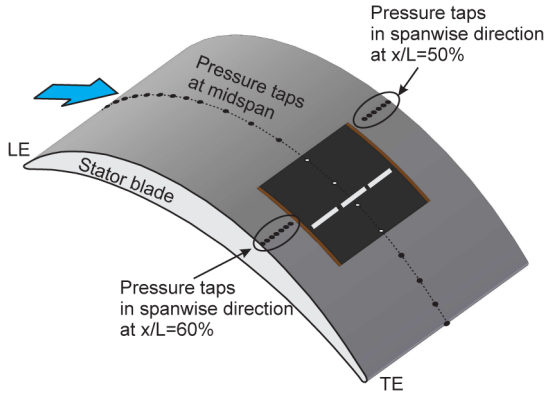

Fig. 5 Instrumentation of the stator blade.

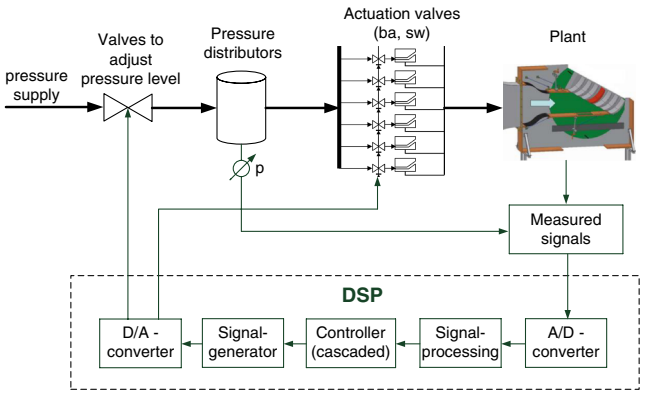

Fig. 6 Schematic diagram of signal flow in closed-loop control experiments.

$$F^{+} = \frac{f \cdot L}{u_1} \tag{2}$$

Corresponding to Fig. 4 this results in a reduced forcing frequency of $F^{+} = 0.43$ (40 Hz) and $F^{+} = 1.28$ (120 Hz) for both actuator concepts. Furthermore, the distance between the injection location and the blade trailing edge should be used as the reference length for the blade actuators, as suggested by Nishri and Wygnanski [20]. Using the local velocity u of the passage flow at the actuator slot position, it results in a normalized forcing frequency of $F^{+}_{\mathrm{BA}} = 0.22$ (40 Hz) and $F^{+}_{\mathrm{BA}} = 0.65$ (120 Hz).

In the present investigation the actuators are driven in phase. The momentum coefficient is individually adjusted for the sidewall and blade actuators.

C. Measurement System

The measurement system used for the experimental investigation has to fulfill two requirements. First, the experimental measurement setup should help to evaluate the passage flowfield and the interaction of periodic excitation with the separated flow. Therefore, different measurement methods were applied in open-loop control experiments, e.g., particle image velocimetry (PIV), wake flow measurements using a five-hole probe, and static pressure taps on the stator blade. All data were recorded during these investigations and analyzed after the data acquisition to obtain a database of forcing parameters for optimal suppression of the flow separation. A more detailed description of the measurement techniques used for open-loop control experiments can be found in previous publications [15,21,22].

Secondly, for the conduction of closed-loop control experiments the most important prerequisite is real-time capability of the applied measurement system. For this purpose fast-responding sensors and a digital signal processor (DSP) are applied cf. Figures 5 and 6, respectively. In the following, the setup that was used for the closed-loop control experiments is described in detail.

1. *Pressure Taps*

The center stator blade of the cascade is equipped with static pressure taps on the suction and pressure side, as shown in Fig. 5. The local static pressure p_x along the blade's surface at discrete positions can be quantified. Fast-responding miniature differential pressure sensors (*SensorTechnics, RMOH*) are placed directly below the blade's surface. The frequency response of the pressure sensors in combination with the pressure taps is constant up to 500 Hz. Along the midspan of the stator blade 30 pressure taps are installed, 19 taps placed on the suction side, 10 on the pressure side, and one pressure tap on the trailing edge (TE) of the blade. Additionally, static pressure taps are placed at two different chord positions ($x/L = 50\%$ and $x/L = 60\%$) in spanwise direction. All static pressure information can be measured simultaneously with an appropriate data acquisition system such as the DSP. Therefore the output signal (25 mV, full-scale span) of the pressure sensor is amplified to $U_{\mathrm{out}} = \pm 5$ V. The typical nonlinearity and hysteresis for this sensor is $\pm 0.25\%$ of the full span scale. The static pressure of the inlet velocity p_1 is used as the referential pressure of the static pressure measurements $p_x - p_1$.

2. *Digital Signal Processor (DSP)*

For the implementation of the controller and the online signal processing in the experiment, a digital signal processor (*dSpace* controller board *DS 1005*, A/D converter board *DS 2003*, D/A converter board *DS 2103*) is used. With it, the conversion, and the processing of the measurement data, the calculation of a control signal and the generation of the signals for the jet actuators can be realized in real time [23]. A schematic description of the signal paths is given in Fig. 6.

The actuation amplitude is adjusted by regulating the pressure within the distributors, which are applied shortly before the valves, as explained above. The result of the chosen setup is a cascaded control structure as it is indicated in the block diagram in Fig. 7 where s denotes the Laplacian variable and d the disturbances. The actual control task to drive the system $\mathbf{G}_2(s)$ to desired reference commands $r(t) = y_{\mathrm{desired}}$ and to compensate disturbances is realized by the robust controller $\mathbf{C}_2(s)$. In dependence of the desired reference command values y_{desired} and the measured values of the control variables $y(t)$, the controller $\mathbf{C}_2(s)$ calculates values for the pressure levels supposed to be adjusted within the distributors $\mathbf{G}_1(s)$. For this, classical PI-controllers $\mathbf{C}_1(s)$ are used in an inner control loop. The bandwidth of the inner control loop is significantly higher than the one of the outer loop. For $\mathbf{C}_2(s)$ the inner loop is part dynamic of the plant.

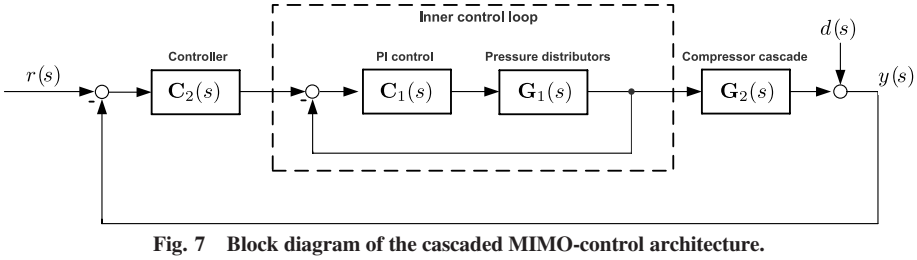

Fig. 7 Block diagram of the cascaded MIMO-control architecture.

III. Controller Synthesis

The physics of a complex process can never be completely covered by a mathematical model. In real environments the control will always have to face uncertainties such as limited process knowledge or immeasurable disturbances. Therefore, a robust control law that guarantees stability under all uncertainties considered is necessary. Even for the worst considered case the process has to be stable in a closed-loop sense. At the same time, robust performance with respect to setpoint tracking and disturbance rejection is desirable, too. To solve this task, a H_∞-design [24] is used here. To obtain a H_∞-controller the so-called mixed-sensitivity problem [25] has to be solved. Within the mixed-sensitivity problem, different requirements concerning the desired closed-loop behavior can be addressed at the same time, such as stability and performance. Frequency dependent weight functions are exploited to define requirements concerning the desired setpoint tracking behavior and disturbance attenuation, as well as actuator limitations. All these requirements are integrated into one cost functional. By minimization of this cost functional, an optimal H_∞-controller can be built. This leads to a controller in such a way that a compromise between robust stability, disturbance rejection and spent energy is obtained. Hence, both stability and performance are addressed.

To synthesize the controller, a mathematical model describing the process and the uncertainty needs to be derived. By various representative step experiments throughout the whole operating range, a set of black-box models, a so-called model family, is identified here. Prediction-error methods [26] are used to identify black-box models that describe the input/output behavior of the system. Compared with the quite complex three-dimensional flow conditions within the compressor cascade, the derived models are rather simple. Models of first or second order are sufficient to describe the essential dynamic behavior of the output values. Based on the identified model family, a middle nominal model with a minimal deviation over the whole frequency range and an uncertainty description can be derived. Practically, this uncertainty description can be interpreted as a measure for the uncertainty of the nominal model.

The proposed control method has already been successfully applied to other flow control configurations [23,27–29]. More information about this approach can be found in standard textbooks, e.g., [25].

IV. Results

A. Base Flow

The high turning of the stator blades, in combination with the small blade aspect ratio of AR = 0.8 causes strong secondary flow structures with additional boundary-layer separation on the blade's suction side. As an example of the complexity of the passage flowfield, the corner vortex is shown in cross-planes in Fig. 8, observed with a stereoscopic PIV setup. An oil-flow visualization of the base flow on the suction surface is shown for comparison. The corner vortex formation and the three-dimensional separation line can be clearly seen.

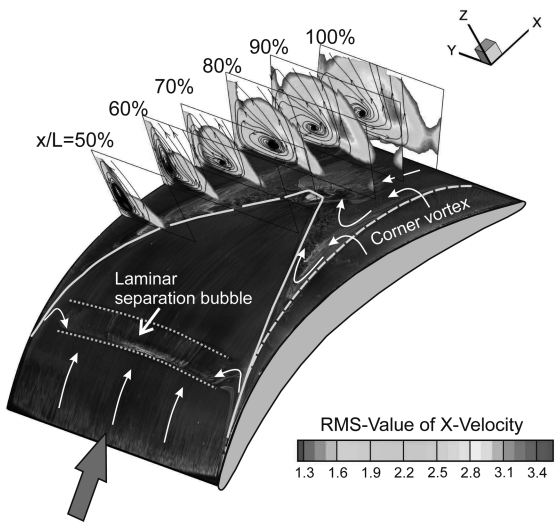

Fig. 8 Oil-flow visualization of the stator blade's suction surface, in combination with PIV measurements of the corner vortex.

Beginning at the leading edge a laminar boundary layer develops, followed by a laminar separation bubble. Along this transition bubble the boundary layer becomes turbulent and reattaches to the blade's surface. A pressure-induced boundary-layer separation occurs at midspan of the suction surface. The flow separates between 70 and 75% chord length (see also Fig. 12a). The well defined three-dimensional separation line is narrowed down by the strong corner vortices. They start in the region of the suction peak and constrict the passage flow downstream. The cross-planes of the corner vortex (see Fig. 8) show the downstream expansion, which results in a high blockage of the passage flowfield. A region of recirculation is indicated by the accumulation of oil paint between the separation line and the corner vortex.

B. Open-Loop Experiments

Two actuator concepts are used to suppress the secondary flow structures and the pressure-induced flow separation. This results in an enhanced turning and diffusion through the stator passage and a reduction of pressure losses. The actuator mechanisms in the flowfield and the impact to the respective flow feature will be described in this section. These results are obtained in open-loop experiments.

1. Sidewall Actuators

The blockage of the passage flow is reduced by repositioning the corner vortices with the use of the sidewall actuators. Figure 9 shows a cross section of the corner vortex at $x/L = 60\%$, obtained by stereoscopic PIV measurements. For comparison, the corner vortex is shown for the base flow and the forced flow case. A forcing frequency of $f_{SW} = 100$ Hz ($F^+ = 1.07$) and a duty cycle of DC = 50% are used. When comparing both flow cases, the vortex moved toward the sidewall with pulsed blowing out of the sidewalls. Also the region of recirculation, indicated by an area of low velocity on the suction surface of the blade, is shifted toward the sidewall. The passage flow, which is unaffected by the secondary flow structures, is represented by the region enclosed by the isoline $u_x = 23$ m/s (black dotted line). Actuation causes an enlargement of this area by decreasing the expansion of the corner vortex. Hence, a reduction of the passage blockage is obtained. This results in a decreased total pressure loss, as well as an increased turning across the passage of the compressor cascade.

The position of the corner vortex is also in good agreement with the spanwise pressure distribution, which is shown below the velocity fields in Fig. 9. Using this pressure information, the position of the corner vortex can be estimated. This information is accessible in real-time needed for closed-loop control. A parameter representing the vortex position can be calculated out of the four marked sensor positions (circle), as described below.

The influence of the forcing frequency on the corner vortex and its position can be seen in Fig. 10. Four phase-averaged pressure distributions at different phase angles (0, 90, 180, and 270°) of the actuator cycle are shown for two different forcing frequencies. For comparison the time-averaged base flow pressure distribution is plotted. At a forcing frequency of 40 Hz (Fig. 10a) the corner vortex is switching between two extreme cases, 90 and 270° phase angle. The 90°-case corresponds to steady blowing (data not shown) and 270° to the base flow, see Fig. 10. This causes a very unsteady behavior of the complete flow in the stator passage. Using a forcing frequencies of 100 Hz (Fig. 10b), the corner vortex position is more stable. The pressure distribution is not changing significantly along the actuator cycle. Thus, using a forcing frequency for the sidewall actuators, which is above the flapping frequency of the vortex system ($f_{SW} \geq 80$ Hz), the blockage can be significantly reduced by means of periodic excitation.

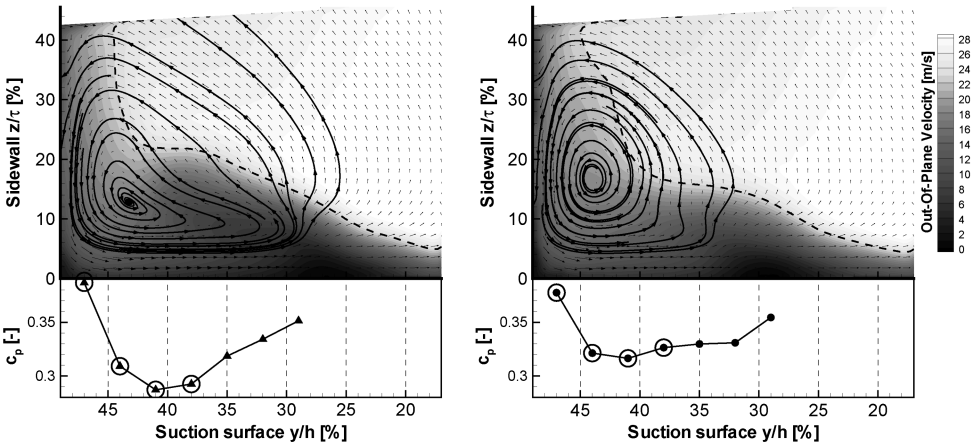

a) Base flow b) Forced flow

Fig. 9 Time-averaged velocity fields of the corner vortex at $x/L = 60\%$ and the spanwise c_p-distribution for the base flow case and with the activated sidewall actuator, running at $f = 100$ Hz ($F^+ = 1.07$) and DC $= 50\%$.

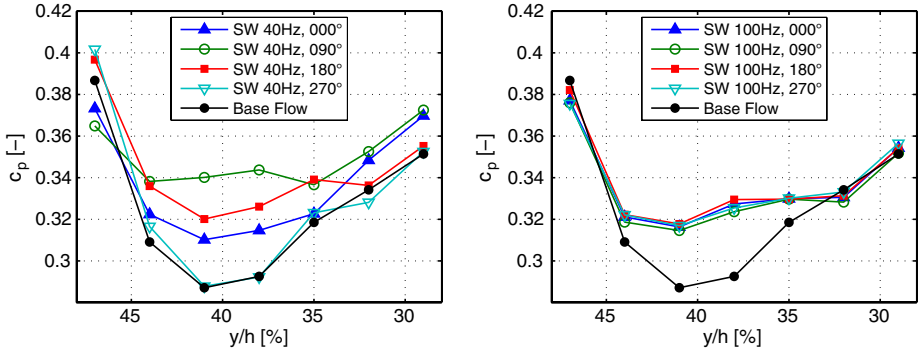

a) Forcing frequency: 40 Hz b) Forcing frequency: 100 Hz

Fig. 10 Phase-averaged pressure distribution at $x/L = 60\%$ in spanwise direction, for forcing frequencies of a) 40 Hz ($F^+ = 0.43$) and b) 100 Hz ($F^+ = 1.07$), respectively, as well as for the base flow case.

Because of the increased turning, the diffusion through the stator passage is enhanced. This results in a static pressure rise $\Delta c_{p,\mathrm{TE}}$, which can be observed at the trailing edge of the blade (cf. Fig. 11).

2. *Blade Actuators*

The pressure-induced boundary-layer separation is suppressed with the actuators on the suction surface of the stator blades. The wall jet forces the separated flow to reattach to the contour of the blade. Figure 12 shows the time-averaged velocity fields of the base flow and the forced flow with the pulsed wall jet. The measurements were

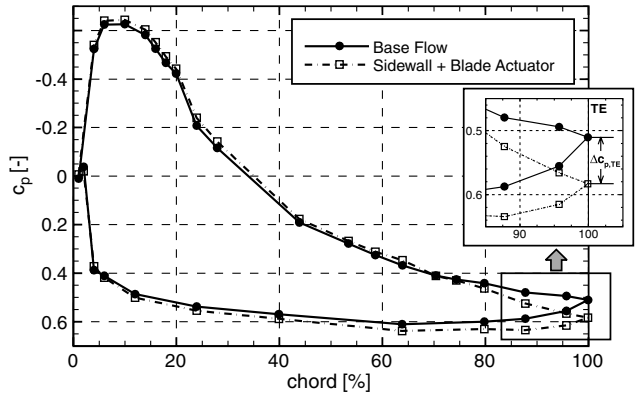

Fig. 11 Pressure distribution at midspan for the base flow case and with actuation. A detailed view shows the static pressure rise at the trailing edge $\Delta c_{p,\mathrm{TE}}$.

carried out using PIV at midspan of the blade. In Fig. 12a) the position of the flow separation can be observed between 70 and 75% chord length. The suppressed flow separation can be clearly seen in Fig. 12b). Because of the pulsed wall jet, high momentum fluid is transferred to the blade surface. The separation line is shifted toward the trailing edge and the blade's turning is enlarged.

Phase-averaged velocity fields out of PIV measurements are used to explain the forcing mechanism of the blade actuator in detail. Figure 13 shows three time-steps $t = 1/10T$ of the actuator blowing cycle T. In that figure, the vorticity induced by the wall jet is color coded, isolines are indicating the absolute velocity between $\mathbf{u} =$ 10 m/s and 25 m/s and vectors are illustrating the velocity field. A counter-rotating vortex pair is developed with the initial blowing phase of the wall jet. This vortex pair is moving downstream with the passage flow (cf. Fig. 13a). The clockwise vortex (white) is quite concentrated, while the counterclockwise vortex (black) dissipates and transfers high momentum fluid to the blade's surface. In Fig. 13b the jet attaches to the wall and is stabilizing the separated boundary layer. At the beginning of the actuator off-cycle (Fig. 13c) the vortex pair breaks down and the region of low fluid momentum is shifted further toward the trailing edge. Upstream of the vortices the boundary layer is still attached to the blade's surface and is stabilized until the next blowing cycle starts. The resulting time-averaged velocity field with the suppressed flow separation, using the same actuator parameter, was already shown in Fig. 12b). Moreover, the separated shear layer has a certain receptivity to this forcing frequency. Using a low forcing frequency, e.g., 40 Hz, the separation is suppressed periodically with the blowing phase. The flow attaches to the blade surface and starts to separate during the actuator off-cycle. So, the best reduction in losses can be obtained with a forcing

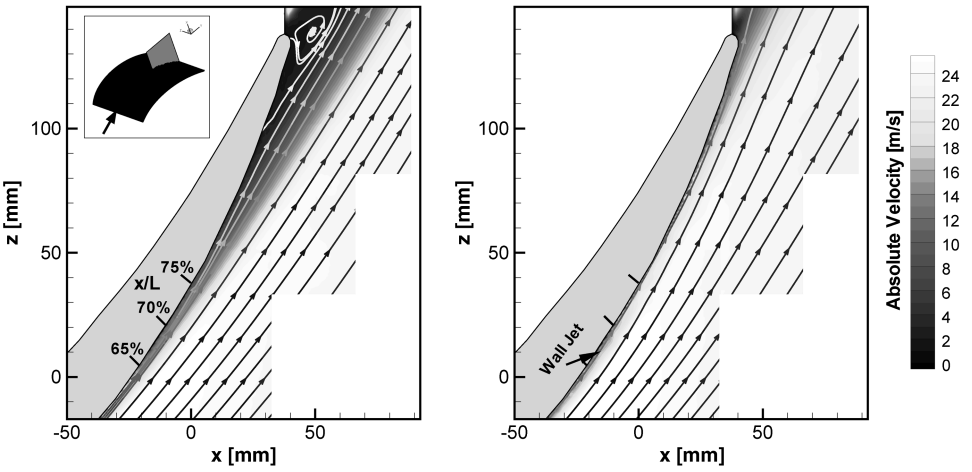

a) Base flow b) Forced flow

Fig. 12 Time-averaged velocity fields of the pressure-induced flow separation at midspan of the blade for the base flow and the forced flow case.

frequency above $F^+ > 0.5$, but the highest static pressure rise at the blade's trailing edge was reached using a forcing frequency of 40 Hz ($F^+_{\mathrm{BA}} = 0.22$) (cf. results in [15]).

By suppressing the pressure-induced boundary-layer separation with the blade actuators, the turning of the blade is significantly increased. This results in an enhanced diffusion across the stator passage, which can be seen in a pressure rise at the trailing edge. This static pressure rise $\Delta c_{p,\mathrm{TE}}$, based on the natural flow case (cf. Fig. 11), is a well-suited parameter estimating the actuator performance. It is used for the open-loop experiments, as well as for the closed-loop control experiments.

3. *Combined Actuation*

The aim of this investigation was to reduce the pressure losses of the stator cascade and the suppression of flow separations in the passage flowfield of the critically loaded compressor blades. This can be achieved using both actuator concepts in combination. With the sidewall actuators the corner vortices are shifted toward the sidewalls and the blockage of the passage flow is reduced. This leads to a decreased total pressure loss $\zeta_{V1} = (p_{t1} - p_{t2})/q_1$ and a static pressure rise $\Delta p/q_1 = (p_2 - p_1)/q_1$ across the stator passage cf. Fig. 14. Additionally, the region of the pressure-induced boundary-layer separation at midspan is enlarged in spanwise direction. With that, the blade actuators can suppress this flow separation more efficiently. The diffusion of the passage increases significantly, using both actuator concepts in combined operation.

Figure 14 represents the gain of the cascade performance using both actuator concepts, obtained by wake flow measurements at one third of the chord length behind the stator blade's trailing edge. The additional injected mass through the actuators into the passage flow is compensated using the correction method described by Hartsel [30]. The pitchwise averaged total pressure loss and the static pressure rise along half of the blade span (midspan: $y/h = 0\%$, sidewall: $y/h = 50\%$) is depicted in both diagrams for the base flow and the actuated flow. Integrating the entire area between both flow cases, the reduction of the total pressure losses (Fig. 14a) and the gain in static pressure rise (Fig. 14b) can be determined. As an example, for one of the best actuator parameter combinations ($f_{\mathrm{SW}} = 150$ Hz, $c_{\mu,\mathrm{SW}} = 0.6\%$ and $f_{\mathrm{BA}} = 120$ Hz, $c_{\mu,\mathrm{BA}} = 0.85\%$), the gain in the static pressure rise is up to 9% and the total pressure loss is reduced by 13%.

The gain of the pressure coefficient at the trailing edge $\Delta c_{p,\mathrm{TE}}$ using both actuator concepts in combination is shown in Fig. 15 for selected actuator parameter. The blade actuators are operated varying the actuator amplitude $c_{\mu,\mathrm{BA}} = 0 \ldots 1.8\%$ at two different forcing frequencies and a duty cycle of 50%, as well as with steady blowing. The sidewall actuators are driven with a constant actuator momentum of $c_{\mu,\mathrm{SW}} = 0.52\%$ at a forcing frequency of $f_{\mathrm{SW}} = 150$ Hz (DC = 50%) and an actuator momentum of $c_{\mu,\mathrm{SW}} = 0.93\%$ with steady blowing. The best gain of the pressure rise $\Delta c_{p,\mathrm{TE}}$ can be reached with a forcing frequency of $f_{\mathrm{BA}} = 40$ Hz in combination with steady blowing out of the sidewalls. When using a forcing frequency of $f_{\mathrm{BA}} = 120$ Hz a slightly higher amplitude is required to

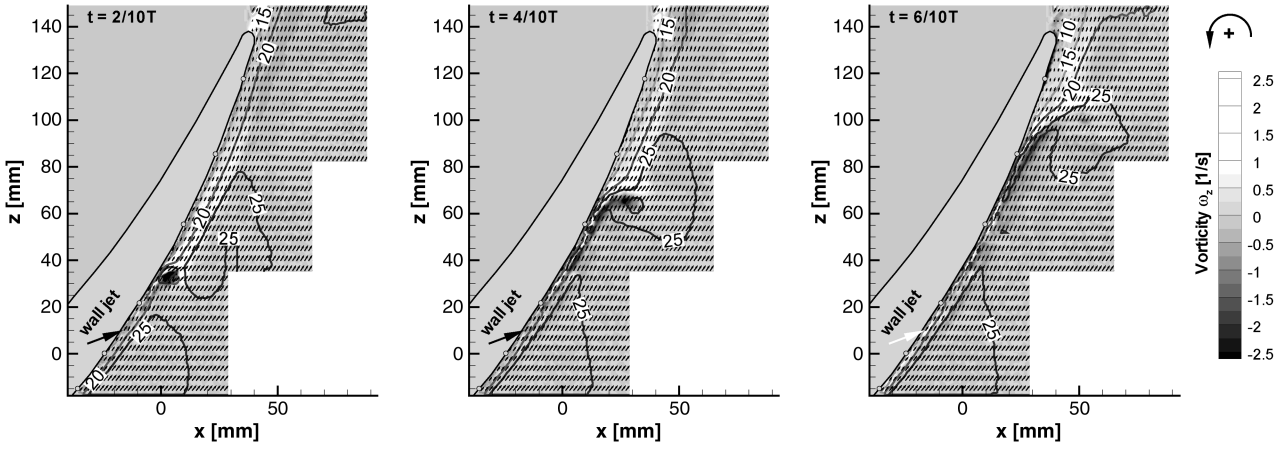

a) b) c)

Fig. 13 Phase-averaged velocity fields with color coded vorticity induced by the wall jet. The actuator's parameters are $f = 120$ Hz ($F^+_{\mathrm{BA}} = 0.65$), DC = 50%, and $c_\mu = 0.92\%$ in this example.

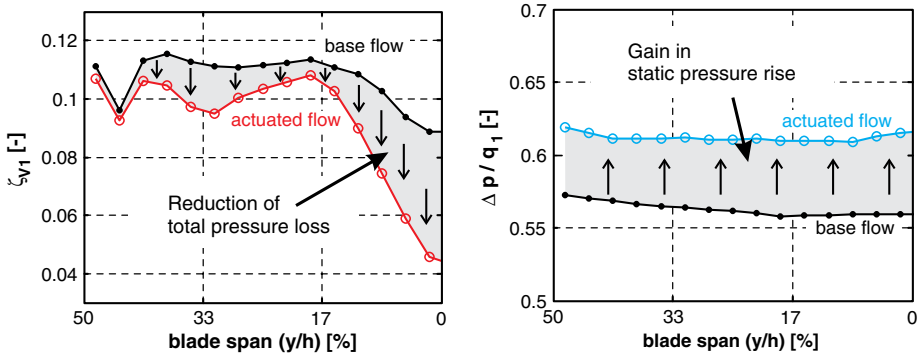

a) Total pressure loss **b) Static pressure rise**

Fig. 14 Wake flow measurements using a five-hole probe: a) reduction of the total pressure loss ζ_{V1}, and b) gain in static pressure rise $\Delta p/q_1$ across the stator passage.

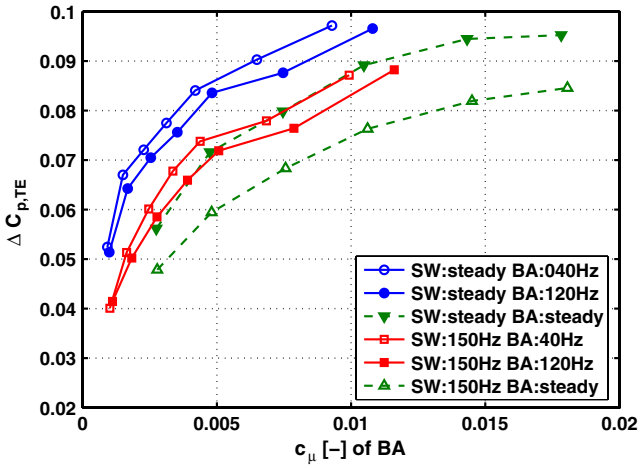

Fig. 15 Combination of both actuator concepts. The pressure rise at the TE is plotted dependent on the momentum coefficient of the blade actuator. Sidewall actuators are driven with pulsed ($c_{\mu,\mathrm{SW}} = 0.52\%$) and steady ($c_{\mu,\mathrm{SW}} = 0.93\%$) blowing.

reach the same pressure rise. Attention should be paid to the actuator momentum of the sidewall actuators, using steady blowing. It is nearly twice the momentum coefficient obtained when using pulsed blowing. Thus, the pressure rise for periodic excitation out of the sidewalls in combination with pulsed blowing out of the blade actuators is lessened.

With steady blowing out of the blade actuators the static pressure gain seen above cannot be improved. For all combinations and momentum coefficients, the pressure rise at the trailing edge is significantly lower.

C. Closed-Loop Control

1. *Derivation of a MIMO-Control Task*

To control both dominant separation phenomena simultaneously, two suitable surrogate control variables have to be defined. They have to be accessible in real-time and should represent important aspects of the process dynamics.

The static pressure rise at the trailing edge $\Delta c_{p,\mathrm{TE}}$ is a possible candidate expressing the pressure enhancement of the stator passage cf. Sec. IV.B. Additionally, the PIV data in Fig. 9 indicate that the spanwise pressure distribution at $x/L = 60\%$ is unambiguously connected to the movement of the corner vortices towards the sidewalls. With actuation, i.e., with a shifted corner vortex, a much flatter pressure profile is obtained giving rise to a smaller spanwise gradient. Exploiting this, four pressure sensors are inserted at 47, 44, 41, and 38% of the blade span to define a second control variable, see as well Fig. 16. A spanwise pressure difference Δc_p is defined as follows:

$$\Delta c_p = (c_{p,47} - c_{p,44}) + (c_{p,47} - c_{p,41}) + (c_{p,47} - c_{p,38}) \qquad (3)$$

The second control variable $\Delta c_{p,\mathrm{spw}}$ is defined as the difference between the actuated case $\Delta c_{p,\mathrm{act}}$ and the base flow case $\Delta c_{p,0}$:

$$\Delta c_{p,\mathrm{spw}} = \Delta c_{p,\mathrm{act}} - \Delta c_{p,0} \qquad (4)$$

With regard to applicability within jet engines it has to be mentioned that the same qualitative signal can be achieved by only using the sensors at 47 and 38% blade span. By using four sensors the signal becomes more accurate and less filtering is necessary.

The influence of both actuators at the sidewall and the blade upon the two control variables is shown in Fig. 17. The left plot shows that both actuators have a significant impact on the gain in static pressure at the trailing edge, though the influence of the blade actuator is stronger.

By pushing the corner vortices outward the spanwise pressure distribution gets more flat cf. Fig. 9, and the pressure difference decreases. The change in the spanwise pressure difference compared with the unactuated case can be seen in Fig. 17b). While a decreasing value of $\Delta c_{p,\mathrm{spw}}$ indicates that the sidewall actuators push the vortices to the sidewall, it is observable that the blade actuators even have a negative effect on this value, although this influence is nearly negligible compared with the impact of the sidewall actuators. Nevertheless, Fig. 17 shows that the stator cascade exploiting two actuators consists of a MIMO process for which an appropriate control approach is needed as the already mentioned H_∞-design. The actuation frequencies chosen are $f_{\mathrm{BA}} = 40$ Hz for the blade actuators and $f_{\mathrm{SW}} = 120$ Hz for the sidewall actuators, each with a fixed duty cycle of 50%.

In the sequel, the actuation amplitude is given in a normalized manner referred to a maximal pressure of $p_{d,\max} = 6$ bar within the distributors cf. Fig. 4.

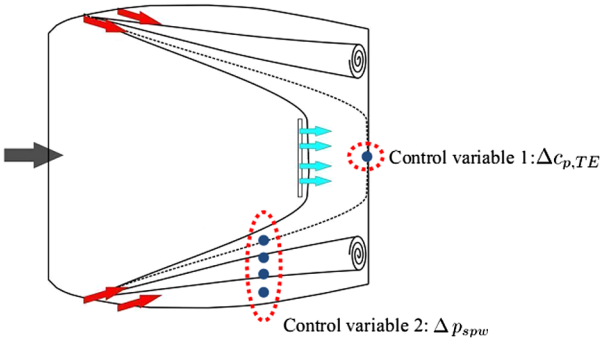

Fig. 16 Schematic view of the derived control variables.

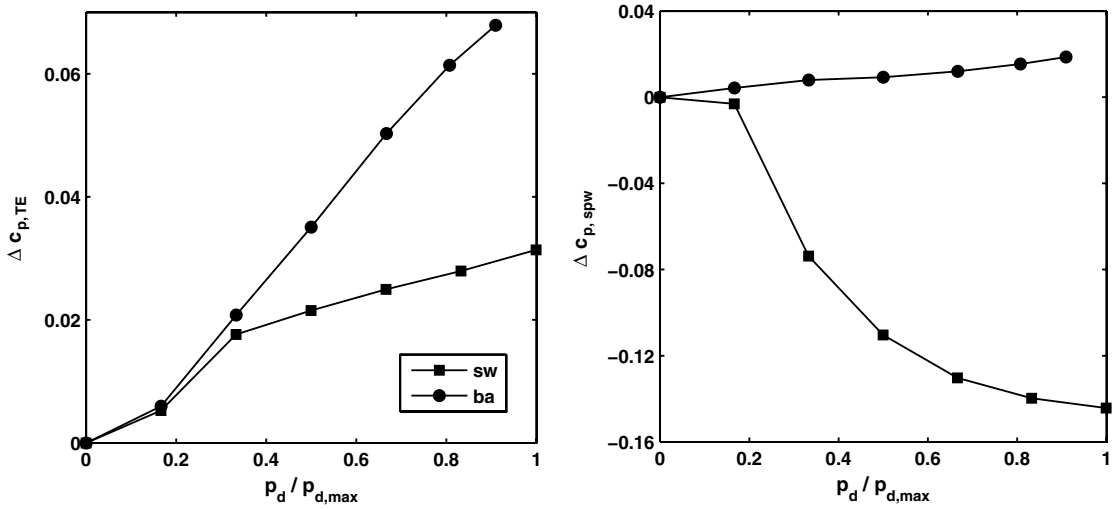

a) Static pressure rise at the TE **b) Spanwise pressure difference**

Fig. 17 Static map of control variables: a) $\Delta c_{p,\mathrm{TE}}$, and b) $\Delta c_{p,\mathrm{spw}}$ as a function of the normalized applied pressure at the blade- and sidewall actuators cf. Fig. 4.

2. MIMO Results

The first closed-loop control experiment conducted is shown in Fig. 18. On the left side both control variables are given. Each is supposed to follow different reference commands $r(t)$ given by the broken line. The obtained setpoint tracking behavior is satisfactory, each reference value for both control variables can be reached without constant errors or overshooting responses. The high frequency oscillations seen are not captured by the models used for controller synthesis. They cannot be controlled either. Therefore, the outputs follow the references in some time-averaged sense.

At $t = 50$ s a first disturbance is simulated by shifting the inlet angle of the compressor cascade to $\beta_1 = 62°$. Through this higher turning the capability of the test rig to build up pressure at the trailing edge rises. Simultaneously, the corner vortices further extend towards midspan. As a consequence, the controller increases the amplitude of the sidewall actuators, while the blade actuators have to force less strongly. By the fast reaction of the controller, this disturbance can be compensated very quickly and almost no effect is observable within the measured values of both control variables.

In contrast to the latter disturbance, at $t = 80$ s the inlet angle is decreased down to $\beta_1 = 58°$. Concomitantly, the capability of the stator passage to build up pressure decreases and the corner vortices stay closer to the sidewall. As a result, the sidewall actuation is significantly reduced by the closed-loop controller, which has an indirect impact on the pressure at the trailing edge, as well. This time the blade actuation has to be increased significantly to drive the system back to the desired reference commands.

To challenge the controller a heavy inlet distortion, simulated by shifting the inlet angle, is introduced next to every reference command, see Fig. 19. This time, the control variables are supposed to follow both reference commands $r(t)$. In Fig. 19, the reference commands $r(t)$ change every 30 s. For each reference value the inlet angle β_1 is shifted very fast every 10 s, as indicated in the lower right panel of Fig. 19.

Again the coupled nature of the passage flow becomes apparent. At $t = 5$ s, β_1 is decreased by about 2°. As explained above, the sidewall actuators reduce their effort, because the corner vortices are developed less strongly. The blade actuators, however, have to compensate the pressure drop by the decreased turning angle and the weaker influence of the sidewall actuation. If now the inlet angle is increased by $\Delta\beta_1 = +4°$ at $t = 15$ s, the limits of this approach are reached. By a higher loading of the blades the pressure at the trailing edge rises while the corner vortices develop more intensely. To avoid that, the sidewall actuators have to interfere, which has an additional effect on the first control variable $\Delta c_{p,\mathrm{TE}}$. As a consequence, even with completely closed valves at the blade, the desired reference

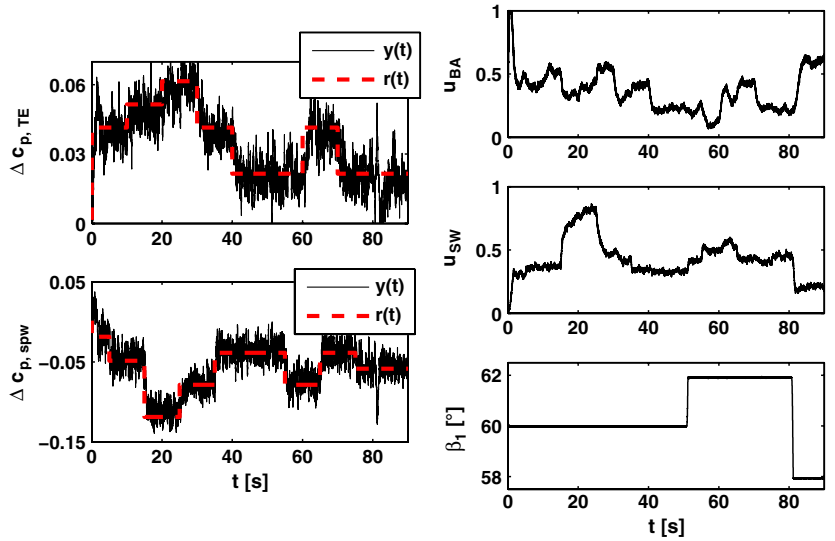

Fig. 18 MIMO closed-loop control with simulated disturbances. The actuation is given in normalized form $u_{\mathrm{BA}} = (p_d/p_{d,\max})_{\mathrm{BA}}$ and $u_{\mathrm{SW}} = (p_d/p_{d,\max})_{\mathrm{SW}}$ cf. Fig. 4.

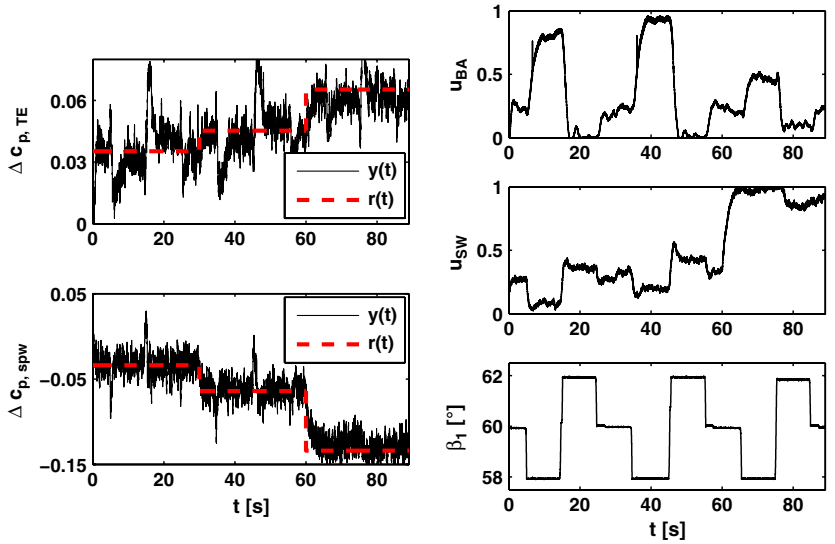

Fig. 19 MIMO closed-loop control experiment under heavy inlet angle distortions.

command is difficult to achieve. Thus, there is a limitation in the proper choice of the desired reference commands, as their corresponding physical phenomena within the cascade are coupled. It is not possible to push the corner vortices closer to the wall and decrease the pressure at the trailing edge at the same time. This can be seen for all reference values given in Fig. 19. From this it follows that the desired control goals have to be chosen in a well set manner.

Moreover, a second limitation has to be pointed out in the control experiments shown. While in the base flow case homogenous inlet flow conditions are adjusted by a time-consuming adaptation of the boundary-layer suction, the flow conditions are no longer well defined under disturbed circumstances. As it is the very nature of disturbances to be unpredictable in a way, it can be regarded as an additional challenge for the controller.

V. Conclusions

Experimental investigations of two different AFC concepts were performed on a critically loaded compressor cascade. Because of the complex passage flow structures, two actuator concepts had to be adapted to the dominant separation phenomena. Pulsed blowing out of the sidewalls was used for suppression of secondary flow structures. The pressure-induced boundary-layer separation in the rear part of the blade could be suppressed by means of pulsed excitation out of slots in the blade's suction surface. With both actuator concepts in combination, the turning of the blade could be increased and the blockage of the passage flow was reduced, resulting in an increased static pressure rise and decreased total pressure loss across the stator passage.

Systematic studies of the actuator parameter, such as the excitation frequency, the jet amplitude, and the duty cycle for both actuator concepts, were performed in open-loop experiments. It was shown that the corner vortex position correlates with the reduction of the passage blockage, which could be estimated by the spanwise pressure distribution. The local mechanisms of the reattachment process of the flow separation were shown by means of PIV measurements. The comparison of the pressure data with the flowfield results demonstrated that the static pressure rise at the trailing edge $\Delta c_{p,\mathrm{TE}}$ is a well-suited parameter for estimating the actuator performance. Using this parameter, the performance of both actuator concepts driven in combination was observed. The static pressure rise at the trailing edge was basically dependent on the actuator momentum and slightly on the actuator frequency. Compared with steady-state blowing, a distinct increase in the cascade performance was reached by pulsed excitation. Choosing suitable actuator parameters for both concepts, a static pressure rise of 8–9% and a reduction in pressure losses of up to 13% were obtained. The required mass flow for both actuator concepts in this combination was about 0.5% of the passage mass flow, which fulfills the industrial limits of additional bleed air consumption.

As a further step, closed-loop control experiments were performed. The applied MIMO approaches were capable of controlling both separation phenomena at the same time. Therefore, two suitable control variables were identified that represented the process dynamics and were quickly detectable. With the MIMO-controller enabled, even heavy disturbances could be compensated within certain physical limits. Thereby a stabilization of the operation was achieved.

The effective suppression of both separation phenomena in combination and the successful closed-loop control approaches are essential requirements to bring these concepts closer to an industrial application. Besides that, other major challenges have to be mastered, e.g., the scaling, robustness, and power density of the excitation device, or the decreasing forcing velocity ratio with increasing inlet Mach number. Even if solutions could be found for these fundamental problems, it has to be proven whether such a flow control system is able to generate a net benefit when accounting the costs of the actuator system and the impact to the engine cycle performance. To give substantial answers to these problems, AFC experiments have to be carried out in a multistage axial compressor rig at realistic Reynolds and Mach numbers, and with an integrated excitation device.

Acknowledgments

The results presented were achieved in cooperation with Rolls-Royce Deutschland, Ltd., & Co. KG as part of the Collaborative Research Center 557, Control of Turbulent Shear Flows, at TU Berlin. The project was funded by the Deutsche Forschungsgemeinschaft (German Research Foundation).

References

[1] Lord, W. K., MacMartin, D. G., and Tillman, T. G., "Flow Control Opportunities in Gas Turbine Engines," *Proceedings of Fluids 2000*, AIAA Paper 2000-2234, Denver, CO, USA, 2000.

[2] Wennerstrom, A. J., "Highly Loaded Axial Flow Compressors: History and Current Developments," *Journal of Turbomachinery*, Vol. 112, No. 4, 1990, pp. 567–578. doi:10.1115/1.2927695

[3] Culley, D. E., Bright, M. M., Prahst, P. S., and Strazisar, A. J., "Active Flow Separation Control of a Stator Vane Using Embedded Injection in a Multistage Compressor Experiment," *Journal of Turbomachinery*, Vol. 126, No. 1, 2004, pp. 24–34. doi:10.1115/1.1643912

[4] Culley, D. E., Braunscheidel, E. P., and Bright, M. M., "Impulsive Injection for Compressor Stator Separation Control," AIAA Paper AIAA 2005-3633, 2005.

[5] Bright, M. M., Culley, D. E., Braunscheidel, E. P., and Welch, G. E., "Closed Loop Active Flow Separation Detection and Control in a Multistage Compressor," NASA Tech. Rept. NASA TM-2005-213553, Glenn Research Center, 2005.

[6] Carter, C., Guillot, S., Ng, W., and Copenhave, W., "Aerodynamic Performance of a High-Turning Compressor Stator with Flow Control," AIAA 2001-3973, 2001.

[7] Hergt, A., Meyer, R., and Engel, K., "Experimental Investigation of Flow Control in Compressor Cascades," *Proceedings of ASME Turbo Expo*, ASME GT2006-90415, 2006.

[8] Matejka, M., Safarik, P., Popelka, L., and Nozicka, J., "Influence of Active Methods of Flow Control on Compressor Blade Cascade Flow," *Proceedings of the ASME Turbo Expo*, ASMEGT2008-51109, 2008.

[9] Nerger, D., Radespiel, R., Gümmer, V., and Clemen, C., "Experimental Investigation of Endwall and Suction Side Blowing in a Highly Loaded Stator Cascade," *Proceedings of the ASME Turbo Expo*, ASMEGT2010-22578, 2010.

[10] Seifert, A., Darabi, A., and Wyganski, I., "Delay of Airfoil Stall by Periodic Excitation," *Journal of Aircraft*, Vol. 33, No. 4, 1996, pp. 691–698.
doi:10.2514/3.47003

[11] Greenblatt, D., and Wygnanski, I. J., "The Control of Flow Separation by Periodic Excitation," *Progress in Aerospace Sciences*, Vol. 36, No. 7, Oct. 2000, pp. 487–545.
doi:10.1016/S0376-0421(00)00008-7

[12] Langston, L. S., "Crossflows in a Turbine Cascade Passage," *Transactions of the ASME: Journal of Engineering for Power*, Vol. 102, No. 4, 1980, pp. 866–874.
doi:10.1115/1.3230352

[13] Eroglu, A., and Breidenthal, R., "Structure, Penetration, and Mixing of Pulsed Jets in Crossflow," *AIAA Journal*, Vol. 39, No. 3, 2001, pp. 417–423.
doi:10.2514/2.1351

[14] Petz, R., and Nitsche, W., "Active Separation Control on the Flap of a Two-Dimensional Generic High-Lift Configuration," *Journal of Aircraft*, Vol. 44, No. 3, 2007, pp. 865–874.
doi:10.2514/1.25425

[15] Hecklau, M., Zander, V., Peltzer, I., Nitsche, W., Huppertz, A., and Swoboda, M., "Experimental AFC Approaches on a Highly Loaded Compressor Cascade," *Active Flow Control II*, edited by R. King, NNFM Vol. 108, Springer, New York, 2010, pp. 171–186.
doi:10.1007/978-3-642-11735-0_12

[16] Doyle, J. C., and Stein, G., "Multivariable Feedback Design: Concepts for a Classical/Modern Synthesis," *IEEE Transactions on Automatic Control*, Vol. 26, No. 1, 1981, pp. 4–16.
doi:10.1109/TAC.1981.1102555

[17] Zames, G., "Feedback and Optimal Sensitivity: Model Reference Transformations, Multiplicative Seminorms, and Approximate Inverses," *IEEE Transactions on Automatic Control*, Vol. 26, No. 2, 1981, pp. 301–320.

[18] Mertens, D., Thiele, F., Swoboda, M., and Huppertz, A., "Transition Modeling Effects on the Simulation of a Stator Cascade with Active Flow Control," *ASME Turbo Expo*, ASME GT2008-50697, 2008.

[19] Gmelin, C., Steger, M., Wassen, E., and Thiele, F., "Unsteady RANS Simulations of Active Flow Control on Turbomachinery Blades," *Active Flow Control II*, edited by R. King, NNFM Vol. 108, Springer, New York, 2010, pp. 203–219.

[20] Nishri, A., and Wygnanski, I., "Effects of Periodic Excitation on Turbulent Flow Separation from a Flap," *AIAA Journal*, Vol. 36, No. 4, 1998, pp. 547–556.
doi:10.2514/2.428

[21] Zander, V., Hecklau, M., Nitsche, W., Huppertz, A., and Swoboda, M., "Active Control of Corner Vortices on a Highly Loaded Compressor Cascade," *Proceedings of the 8th European Turbomachinery Conference (ETC)*, Verlag der TU Graz, Graz, Austria, 2009, pp. 41–50.

[22] Hecklau, M., van Rennings, R., Zander, V., Nitsche, W., Huppertz, A., and Swoboda, M., "Particle Image Velocimetry of Active Flow Control on a Compressor Cascade," *Experiments in Fluids*, Vol. 50, No. 4, 2011, pp. 799–811.
doi:10.1007/s00348-010-0895-z

[23] Wiederhold, O., and King, R., "Robust Control in Turbomachinery Configurations," *Active Flow Control II*, edited by R. King, Vol. 108, Springer, New York, 2010, pp. 187–201.
doi:10.1007/978-3-642-11735-0_13

[24] Kwakernaak, H., "Robust Control and H_∞-Optimization: Tutorial Paper," *Automatica*, Vol. 29, No. 2, 1993, pp. 255–273.
doi:10.1016/0005-1098(93)90122-A

[25] Skogestad, S., and Postlethwaite, I., *Multivariable Feedback Control*, Wiley, New York, 1997.

[26] Ljung, L., *System Identification: Theory for the User*, Prentice–Hall, Englewood Cliffs, NJ, 1987.

[27] Becker, R., King, R., Petz, R., and Nitsche, W., "Adaptive Closed-Loop Separation Control on a High-Lift Configuration Using Extremum Seeking," *AIAA Journal*, Vol. 45, No. 6, 2007, pp. 1382–1392.
doi:10.2514/1.24941

[28] King, R., Becker, R., Garwon, M., and Henning, L., "Robust and Adaptive Closed-Loop Control of Separated Shear Flows," *2nd AIAA Flow Control Conference*, AIAA Paper 2004-2529, 2004.

[29] Weigl, H., and Paduano, J., "Application of H_∞-Control with Eigenvalue Perturbations to Stabilize a Transonic Compressor," *Proceedings of the 1997 IEEE International Conference on Control Applications*, IEEE Publications, Piscataway, NJ, 1997, pp. 691–698.
doi:10.1109/CCA.1997.627739

[30] Hartsel, J. E., "Prediction of Effects of Mass-Transfer Cooling on the Blade Row Efficiency of Turbine Airfoils," *10th Aerospace Sciences Meeting*, AIAA 1972-11, 1972.

L. Cattafesta
Associate Editor